# Intramolecularly Hydrogen-Bonded Aromatic Pentamers as Modularly Tunable Macrocyclic Receptors for Selective Recognition of Metal Ions

Ying Liu,[†,⊥] Jie Shen,[‡,⊥] Chang Sun,[§,⊥] Changliang Ren,[‡] and Huaqiang Zeng[*,‡]

[†]Prinbury Biopharm. Co., Ltd, 538 Cailun Road, Zhangjiang Hi-Tech Park, Pudong District, Shanghai, 201203, China
[‡]Institute of Bioengineering and Nanotechnology, 31 Biopolis Way, The Nanos, Singapore 138669
[§]College of Textiles and Clothing, Jiangnan University, 1800 Lihu Avenue, Wuxi, Jiangsu214122, China

**S** *Supporting Information*

**ABSTRACT:** Despite the tremendous progress that has been made in macrocyclic chemistry since the discovery of corands, cryptands, and spherands more than four decades ago, macrocyclic systems possessing a high level of controllability in structural configuration concurrent with a systematic tunability in function are still very rare. Employing an inner design strategy to orient H-bonding forces toward a macrocyclic cavity interior while convergently aligning exchangeable ion-binding building blocks that dictate a near-identical backbone curvature, we demonstrate here a novel pentagonal framework that not only enables its variable interior cavity to be maintained at near-planarity but also allows its ion-binding potential to be highly tunable. The H-bonded macrocyclic pentamers thus produced have allowed a systematic and combinatorial evolution of ion-selective pentamers for preferential recognition of $Cs^+$, $K^+$, or $Ag^+$ ions.
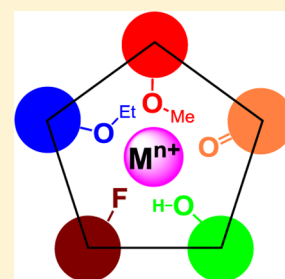
## INTRODUCTION

With the increasingly engendered attention from researchers worldwide over the past five decades since the seminal reports on macrocyclic cation-binding corands by Pedersen,[1a,b] cryptands by Lehn,[1c,d] and spherands by Cram,[1e,f] the notion that macrocyclic chemistry has thus far prospered to become one of the most dynamic and promising frontiers of chemical research, cutting across many traditional scientific boundaries among chemistry, physics, biology, medicine, and engineering seems inescapable. Simultaneous with the innovatively stirring progresses on the cavity-containing functional macrocycles of varying designs and sizes is their highly interdisciplinary applications that involve all sorts of host–guest interactions as a focal entry point into a wide variety of fields including catalysis, environmental remediation, molecular machines, enzyme mimetics, medical diagnostics, and tumor and antiviral therapeutics.

One salient characteristic of macrocyclic hosts is a degree of substantial rigidity that physically confers a particular shape onto the host–guest structure, directly contributing to the enhanced stability over that of the similar acyclic host. Traditionally, this so-called "macrocyclic effect" is mostly derived from the macrocyclic covalent constraints. An elegant strategy that is recently advanced by Hamilton,[2a] Gong,[2b,c] and others[2d–f] explores the conformational preorganization of the folding molecules, i.e., foldamers,[3] using noncovalent intramolecular H-bonding forces, followed by ring-closing reactions to furnish H-bonded macrocyclic aromatic foldamers. In this tactic, every monomer of varying designs to be incorporated into the macrocyclic folding backbone is characterized by its unique H-bond-enforced conformational bias that determines and parametrizes the backbone curvature and macrocyclic cavity. Thus, the cavity-enclosing propensity of these folding macrocycles is mostly independent of the macrocyclic ring constraint. This foldamer-based approach has consistently allowed the efficient creation of sizable interior cavities ranging from 1.4 to 15 Å in radius in the H-bonded macrocycles[2e,f] with a number of them expressing tailor-made functions such as stabilization of G-quadruplex structures,[4a] ion transport,[4b] recognition of ionic[4c–g] or neutral[4h–j] guests, solvent gelation,[4j] reaction catalysis,[4k] and selective demethylation.[4l]

Over the past few years,[2e,f] we have been applying an inner design strategy to systematically develop H-bonded macrocyclic aromatic pentamers, which possess unique aesthetically pleasing five-fold symmetry, in terms of structure,[4e,5] rapid synthesis,[6] and function.[4d–f,j–l] As illustrated by our recently reported intramolecularly H-bonded macrocycles **1−3** respectively built from monomeric methoxybenzene (**A**),[5a] pyridone (**B**),[4e] and fluorobenzene (**C**)[5b] motifs (Figure 1a), our molecular approach features the utilization of a continuous intramolecular H-bonding network that points toward the interior of the macrocycle instead of its exterior. This inner design strategy not only provides the much needed, entropically favorable preorganization force to guide the folding of an otherwise randomly orienting backbone into a defined, rigid conformation but also affords (1) an arrangement of five properly spaced convergently aligned electron-rich donor atoms around an enclosed cavity of 1.4 Å in radius after excluding the volumes of the donor atoms such as O atoms, which is suitable for binding
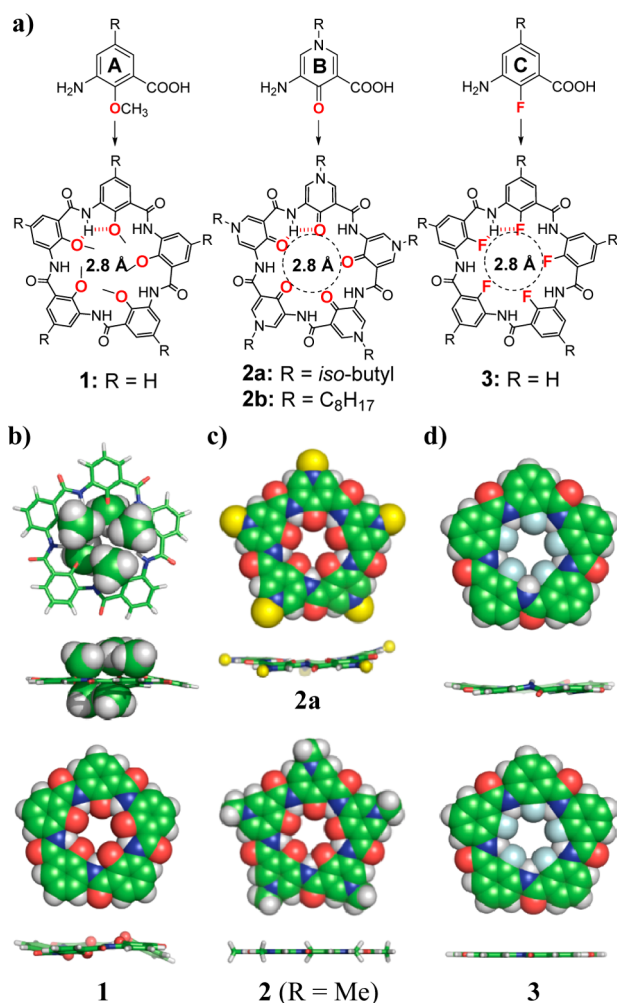
**Figure 1.** Structural features of pentamers **1**−**3**. (a) Structures of pentamers **1**−**3** derived from monomeric building blocks **A**−**C**, respectively, each containing an interior cavity of ~2.8 Å in diameter defined by oxygen or fluorine atoms. (b−d) The top and side views of crystal structures **1**, **2a** and its computationally determined structure as well as **3** and its computationally determined structure. In the bottom of (b), the five interior methyl groups were removed for a unblocked view of a sizable cavity in **1**. The yellow balls in (c) refer to the five exteriorly arrayed *tert*-butyl groups that have been removed for clarity of view. The computationally determined structures for both **2a** and **3** illustrate five-fold symmetry and a planar pentagonic backbone contained in this family of pentamers.



**Figure 2.** (a) Schematic illustration of additional building blocks **D** and **E** for constructing macrocyclic hybrid pentamers such as **4** (b). Amidated trimer as represented by (**B**)$_3$ in (c) was used for calculating $\theta$ values and the number of residues ($n$) required for **A-E** to form a regular pentagon. In (c), angle $\theta$ is defined by the atoms in red as the external angle of a pentagon to be formed, which will be computationally determined by the first principle calculation at the B3LYP/6-31G(d,p) level and compared to the crystallographically derived values.

molecular framework (e.g., the pentameric backbone in this work) has no literature precedents among the hitherto reported ion-binding macrocycles including corands,[1a,b] cryptands,[1c,d] spherands,[1e,f] torands,[7a] or other shape-persistent aromatic macrocycles including porphyrin derivatives or analogues,[7b,c] arylene ethynylene macrocycles,[7d] macrocyclic Schiff bases,[7e] cyanostar macrocycles,[7f] and intramolecularly H-bonded macrocycles.[2d−f]

## ■ RESULTS AND DISCUSSION

**Computational and Crystallographic Determination of Intrinsic Backbone Curvature Associated with Building Blocks A−E.** An enlightened observation from our recent crystallographic studies on pentamers **1**[5a] and **3**,[5b] and current work on the crystal structure of **2a**,[8] reveals a fascinating and intrinsic propensity exhibited by building blocks **A**−**C**; all require five repeating units to form a nearly planar five-residue macrocyclic backbone (Figure 1). This unique feature can be substantiated computationally by the first-principle computations at the B3LYP/6-31G(d,p) level (Figure 1c,d). Nevertheless, in order to eliminate any possible effect the macrocyclic ring constraint might have on the backbone curvature truly intrinsic to the oligomers derived from monomeric building blocks **A**−**C** and other closely related building blocks **D** and **E** (Figure 2a), we focus on the amidated trimers (**A**)$_3$−(**E**)$_3$ with a general structure exemplified by (**B**)$_3$ that comprises three **B**s (Figure 2b) to more accurately determine the intrinsic curvatures solely inducible by these units. On the basis of angle $\theta$ defined by the electron-rich atoms highlighted in red as the external angle of a polygon to be formed (Figure 2b), the number of units ($n$) required to form an idealized polygon free of ring strains can be calculated by using the equation $n = 360°/\theta$.

From the values of $\theta$ and $n$ summarized in Table 1 that were determined from the computationally optimized trimers (**A**)$_3$−(**E**)$_3$ at the B3LYP/6-31G(d,p) level (Figure S1), the methoxybenzene building block **A** is the only one that is perfectly compatible with a regular pentagon and so should produce pentamer **1** that is free of ring strain. Computationally, however, the steric crowding involving the five interior methyl groups destabilizes **1** by 2−3 kcal/mol at the B3LYP/6-311+G(d,p) level,[4k] thus making **1** slightly distorted (Figure 1b). On the other hand, the larger ethyl groups in **D** seem to significantly distort the pentameric backbone (**D**)$_5$ comprising five **D**s (Figure S2a), while the plasticity of the amide bond[2f]

Such as K$^+$ ions (radius = 1.38 Å) and (2) a covalent nanoscaffolding for the expedient exchange of a multitude of modular functional groups that decorate the macrocyclic interior surface. In this regard, our principal motivation has been to design and assemble readily adjustable convergent binding elements around a cavity for the selective recognition of diverse cations. In line with this vision and by using five exchangeable building blocks **A**−**E** (Figures 1 and 2), we now report a novel class of discrete shape-persistent macrocyclic hybrid pentamers, which contain a high degree of precisely tunable interior properties, including effective cavity size, steric crowding, cavity hydrophobicity, and cation-binding capacity for the speedy evolution of ion-selective hybrid pentamers. To the best of our knowledge, a modularly tunable system with such a high degree of controllability in interior property confined within the same type of well-maintained near-planar
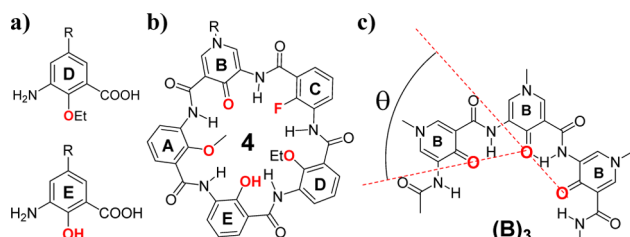
**Table 1. Computationally determined values for $\theta$ and the corresponding number of residues ($n$) required for various building blocks A-E to form a regular pentagon by using computationally optimized amidated trimmers $(A)_3$-$(E)_3$ as represented by $(B)_3$ in Figure 2b and the experimental values obtained from the crystal structures 5a-5e in Figure 3**

| | By Computation[a] | | | | | By X-ray Crystallography | | | | |
|---|---|---|---|---|---|---|---|---|---|---|
| | $(A)_3$ | $(B)_3$ | $(C)_3$ | $(D)_3$[b] | $(E)_3$ | $(A)_3$[b] | $(B)_3$[b] | $(C)_3$[b] | $A(C)_2$[c] | $(A)_2C$[b,d] |
| $\theta$ (deg) | 72.0 | 67.6 | 71.0 | 72.1 | 71.2 | 71.6 | 68.0 | 73.1 | 70.0 | 68.9 |
| $n$ (=360/$\theta$) | 5.00 | 5.33 | 5.07 | 4.99 | 5.05 | 5.03 | 5.30 | 4.93 | 5.14 | 5.22 |

[a]Structural optimizations were carried out at the B3LYP/6-31G(d,p) level in the gas phase, and except for $(D)_3$, all the other trimeric structures were found to take a planar or nearly planar backbone (Figure S1) . [b]The $\theta$ values were obtained by planarizing the slighted twisted backbones in $(D)_3$, 5a,[10a] 5b, 5c, and 5e, respectively. [c]The averaged value over the two $\theta$ values found in tetramer 5d. [d]One of the unit A in 5e contains a benzyl rather than methyl group.
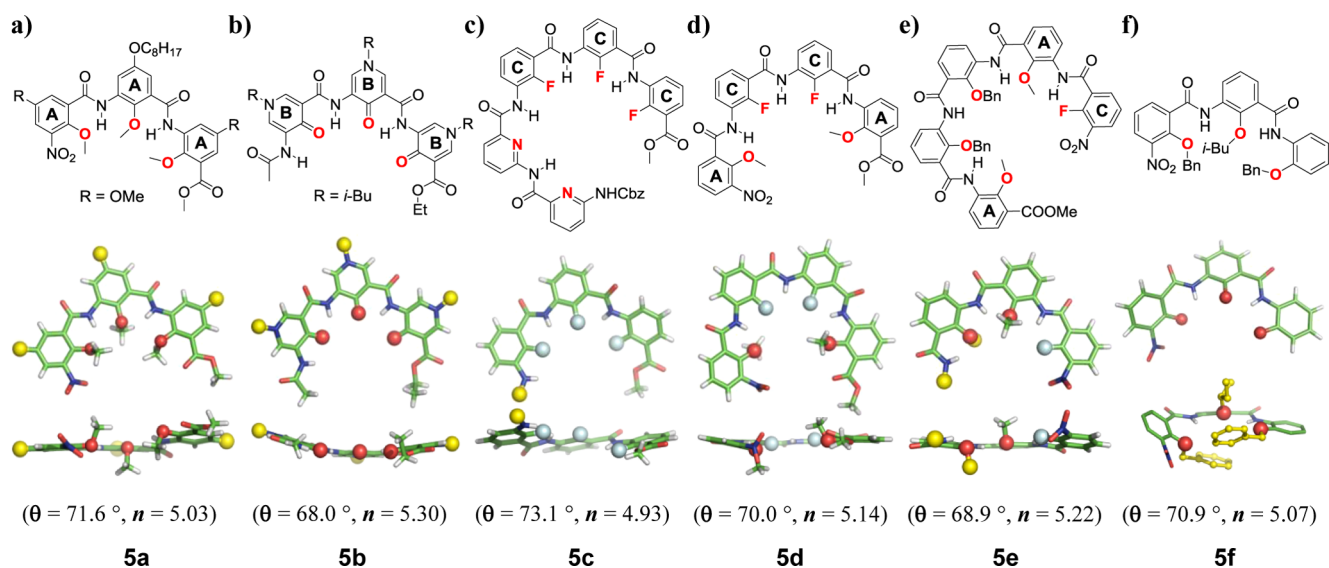


**Figure 3.** Crystallographic verification of computationally determined values of $\theta$ and $n$ listed in Table 1 for H-bonded oligomers 5a-5f that were derived from monomeric building blocks A-C. For clarity of view, exterior side chains, some aromatic building blocks and H atoms were removed. In (a) and (b), the large yellow balls refer to the exterior side chains. In (c), the large yellow ball refers to the bipyridine fragment. In (e), the large yellow balls refer to the fragment at the ester end and the benzyl group. And the smaller yellow balls in (f) refer to the interior benzyl and *tert*-butyl side chains whose H atoms were removed for clarity of view.

enables slightly imperfect units **B**, **C** and **E** to nicely fit into a pentameric framework, producing perfectly planar backbones in **2** and **3** (Figure 1c-d), and nearly planar one in $(E)_5$ (Figure S2b).[9]

The obtained computational results were then subject to scrutiny by X-ray crystallography using crystal structures determined for acyclic oligomers 5a-5f built from units **A-E** (Figure 3). As compiled in Table 1, both $\theta$ and $n$ values for acyclic oligomers 5a-5d are remarkably comparable with the computed values, highlighting high reliability and accuracy of the first principle calculation at the B3LYP/6-31G(d,p) level that has consistently allowed us to predict the structures of a series of analogous H-bond-rigidified foldamer molecules that were verified experimentally later by their crystal structures.[10a] Significantly, the intramolecular H-bonding forces seem to be strong enough to withstand a coexistance of two benzyl groups as in 5e (Figure 3e), or two benzyl and one *iso*-butyl groups as in trimer 5f with a $\theta$ value of 70.9° and $n$ value of 5.07 (Figure 3f).

**Combinatorial Aspect of Macrocyclic Hybrid Pentamers.** On the above computational and experimental grounds and further considering a modular nature of the pentameric backbones, we proposed here an efficient means of generating a rich family of cation-binding hybrid pentamers with a 2D-shaped pentagonic backbone as represented by **4** (Figure 2c).

The underlying molecular strategy involves a combinatorial use of compatible and exchangeable units **A-E** that occupy five circular positions in a pentameric framework. The corresponding library size $N$ can be calculated based on the following equation, whereas **m** is the number of different units used in the library construction.

$$N = \frac{m^5 - m}{5} + m$$

The library size $N$ apparently increases rapidly with an increase in the number of exchangeable units. For instance, 8 and 629 hybrid pentamers can be produced from two and five different units, respectively, and the use of nine different units would quickly lead to 11,817 structures that possibly can be achieved by further incorporating functional groups including pyridine N-oxides, sulfanes,[11a] thiol groups or halogen atoms[11b] into the same pentameric framework (Figure S3).[11c] Thus, a substantial perspective on cation-binding potential becomes readily envisionable on the basis of the following premises: (1) the ion-binding cavity in the hybrid pentamers is tunable between 0 Å as in **1** whose cavity was completed blocked by the five interior methyl groups and ~1.4 Å as in **2** or **3**, while the ionic radius of the majority metal cations falls within 0.6−1.4 Å, (2) the ion-binding interior is decorated by five properly spaced convergently aligned donor atoms in a preorganized manner for

possibly enhanced binding affinity and selectivity, (3) the ion-binding ability of the donor atoms toward metal ions differs significantly among units **A**-**E** with **B** being the strongest, **C** the weakest, and **A**, **D** and **E** as the moderate binders, (4) the methyl and ethyl groups in **A** and **D** are sterically bulky and hydrophobic in nature and may have subtly different orientations, additionally facilitating the fine-tuning of cation-binding affinity and selectivity, (5) under favorable circumstances, the hydroxyl group in **E** might become stronger binders upon a possibly selective deprotonation mediated by certain metal ions, further augmenting the ion binding potential of the system,[10b] and (6) futuristic introduction of additional building blocks (N-oxide, sulfur and halogen atoms, Figure S3) would create similarly sized cavities with higher electron densities, likely endowing the hybrid pentamers with the ability such as to differentiate heavy metal ions from alkali metal ions.

**Crystallographic Aspect of Macrocyclic Hybrid Pentamers.** Toward further characterizing our design, a total of 16 pentamers, i.e., pentamers **6**−**20** (Figures 4 and 5), were
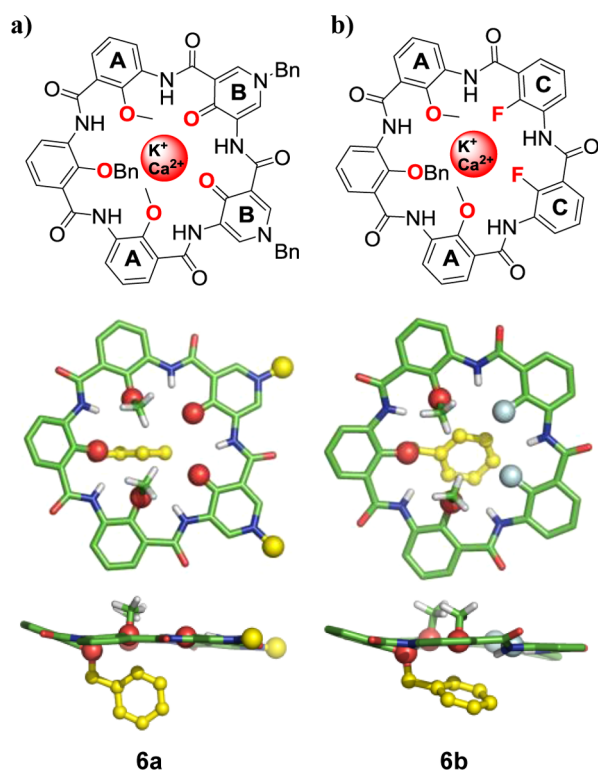


**Figure 4.** Top and side views of crystal structures of **6a** (a) and **6b** (b), demonstrating a near-planar pentagonic backbone that encloses a cavity with a radius of ∼1.4 Å decorated by electron-rich atoms for cation recognition. For clarity of view, exterior benzyl side chains in **6a** were replaced with two dummy yellow atoms, and H atoms in benzyl groups in both **6a** and **6b** were removed. Balls in red and light blue refer to O and F atoms, respectively. The most extractable K⁺ ions and the second most extractable Ca²⁺ ions whose extractability lies within 80% of K⁺ ions are highlighted in the cavity.

synthesized (Scheme S1), and crystallizations were attempted to elucidate the structural features of hybrid pentamers and to evaluate their ability to selectively recognize metal ions. However, obtaining X-ray quality crystals for pentagon-shaped molecules has always been exceptionally challenging. For instance, both X-ray quality crystals for **2a**[8] and **3**[5b] shown in Figure 1c,d took us 2−3 years after trying many different

crystallization conditions containing **2a** or **3** at various concentrations. In particular, crystals for **3** were eventually obtained by slow cooling of a solution containing 1.1 mg/mL of **3** in hot DMSO from 110 to 25 °C at 1° per day over 3 months. Likewise, after countless unsuccessful attempts involving all the 16 pentamers **6**−**20** under various crystallization conditions at various concentrations of pentamers, single crystals of **6a** and **6b** were obtained via extremely slow diffusion of the top methanol layer into the middle layer containing dichloromethane and methanol (1:1, v/v), which subsequently diffuses into the bottom pentamer-containing dichloromethane or chloroform layer at room temperature for a few months. And all the other pentamers failed to yield X-ray quality crystals under the conditions tested. Both pleasantly and excitingly, the determined crystal structures demonstrate a highly sought-after folding of both **6a** and **6b** into an almost planar disk arrangement in solid state with the five electron-rich atoms and amide protons pointing inward to form a continuous intramolecularly H-bonded network. This H-bonding network not only rigidifies the amide linkages but also produces a well-defined, rigid, circularly folded conformation with a pentagon shape, convergently bringing electron-rich donor atoms to enclose a cavity of ∼1.4 Å in radius for potentially selective ion recognition (Figure 4).

**Selective Recognition of Metal Ions by Macrocyclic Hybrid Pentamers.** Our unpublished works reveal no detectable extractions of any metal ion within the instrument's sensitivity by the hybrid pentamers that contain four or five **A**s such as **1**. This implies that the existence of four or more methoxy groups simply imposes too much steric hindrance or hydrophobicity onto the cavity, either blocking the cavity or making pentamers unable to compensate for the loss of hydration energy during the dehydration process when the hydrated cations enter the cavity. Similarly, **3** containing five **C**s poorly extracts any metal ion from aqueous solution to organic phase, confirming the electron-rich fluorine atom with the highest electronegativity as an extraordinarily poor electron donor that can hardly compete with the water molecules in binding aqueous metal ions. In sharp contrast, pentamer **2b** composed of five **B**s (Figure 1a) displays a high-capacity extraction of larger metal ions such as Cs⁺, Ba²⁺, K⁺, and Rb⁺ over the other 14 smaller metal ions.[4f] This high-capacity extraction mostly arises from a greatly enhanced electron density around the O atom from the carbonyl group in **B** as a result of an electron-donating effect from the N atom at the *para*-position in pyridone unit **B** via an aromatic resonance structure in which the N atom is positively charged and the carbonyl O atom carries a negative charge. This resonance effect makes the carbonyl O atom in **B** possess a higher yet donarable electron density than the O atoms found in unit **A**, 18-crown-6 (**21**) and kryptonfix-222 (**23**), which in turn are higher in donarable electron density than the F atom found in unit **C**. Therefore, it is expected that hybrid pentamers **6**−**20** built from units **A**−**E** would bind larger metal ions including Cs⁺, Ba²⁺, K⁺, and Rb⁺ more weakly than **2**, but might have distinctively different selectivity profiles. To examine how the cation-binding function is related to variable interior properties, all the 16 hybrid pentamers **6**−**20** have been tested against 20 metal ions to obtain their ion recognition patterns especially in comparison with **2b** and other oxygen/nitrogen-containing macrocycles **21**−**23** (Figure 5).

In a typical experimental setup using biphasic water−CHCl₃ extraction system of equal volumes, the concentration of each
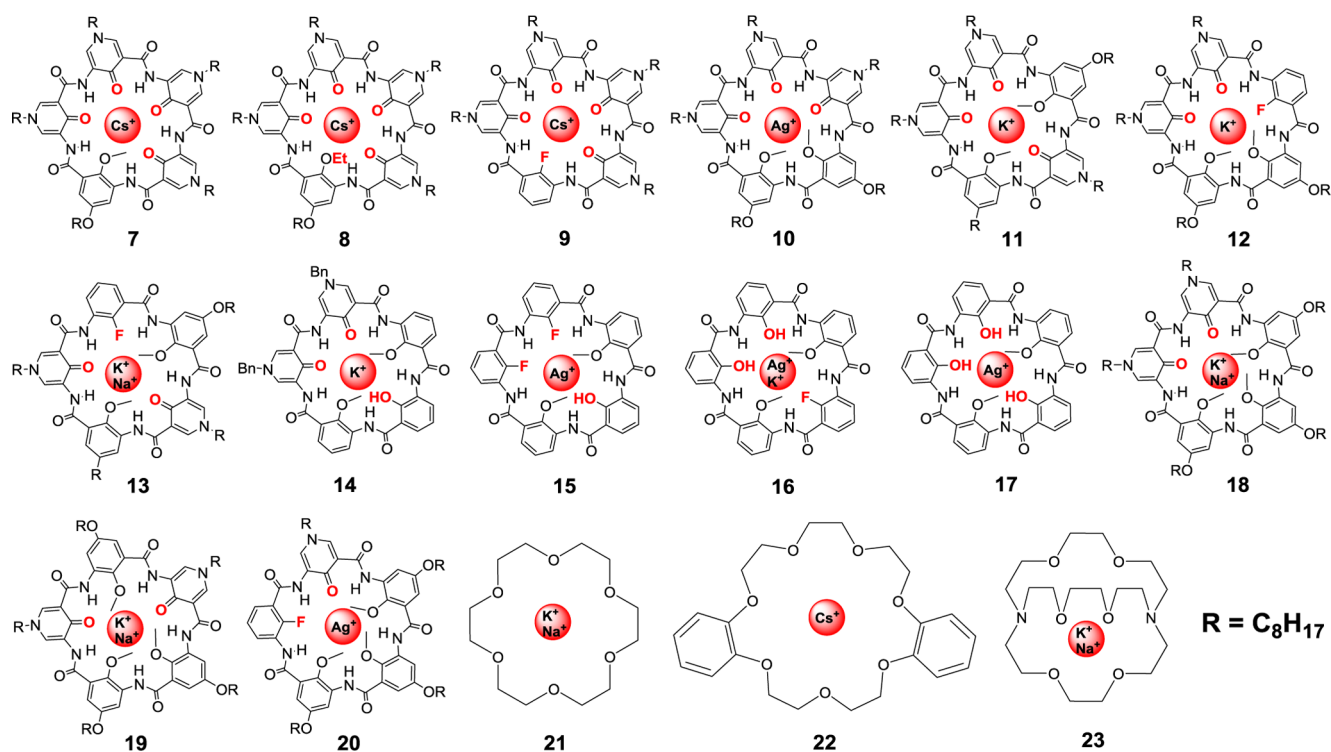
**Figure 5.** Structures of hybrid pentamers **7–20** employed to probe the potential for selective recognition of metal ions by a family of macrocyclic hybrid pentamers with modularly tunable interior properties. The ion-extraction profiles determined under the identical conditions for the three well-known ligands, i.e., 18-crown-6 (**21**), dibenzo-21-crown-7 (**22**), and kryptonfix-222 (**23**), were included for comparison purpose. The ions whose extractability lies within 80% of the most extractable ones are additionally highlighted below the most extractable ones in the cavity.

metal ion in $H_2O$ is set constant at 0.03 mM, and the total concentration for 20 metal ions is therefore 0.60 mM. The concentration of macrocycles in $CHCl_3$ is varied from 0.10 to 1.20 mM. After shaking the biphasic water–$CHCl_3$ solution for 24 h at 25 °C, ion extractions from aqueous phase to chloroform layer were monitored by measuring the residual concentrations of various metal ions in $H_2O$ layer. To ensure that the data obtained are reproducible, the measurements for the same extracted solution were repeated three times, and the whole experiment including preparation of a new batch of sample solutions, extractions, and measurements were repeated one more time. Averaging the data over 6 runs gave the final extraction data with relative errors of ≤3%. From the measured ion-extraction profiles associated with macrocycles **2b** and **6–23** (Tables S1 and S2), important binding information including total ion-extraction capacity, the most extractable ions and the relative extractability among the individual ions can be derived, and are presented in Figure 6.

Consistent with our expectation, an excellent tunability in interior properties indeed imparts experimentally measurable ion-binding selectivity onto these macrocyclic hybrid pentamers **6–20**. Among the 17 pentamers, four (**2b** and **7–9**, Figure 6a) are $Cs^+$-selective, four (**10, 15, 17,** and **20**, Figure 6b) are $Ag^+$-selective, and three (**13, 18,** and **19**, Figure 6b) are $K^+$-selective. Given that the extractability of the second most extractable ion lies within 80% of the most extractable one by the same host (Figure 6b and Table S1), the remaining six pentamers could be considered as having a dual selectivity, including three $K^+$/$Na^+$-selective hosts (**13, 18,** and **19**), two $K^+$/$Ca^{2+}$-selective hosts (**6a** and **6b**), and one $Ag^+$/$K^+$-selective host (**16**). For comparison, hosts **21** and **23** both are $K^+$/$Na^+$-selective, and **22** is $Cs^+$-selective.

In more details, replacing one pyridone unit **B** in **2b** either with one methoxybenzene unit **A** as in **7** or one bulkier ethoxybenzene unit **D** as in **8** or one fluorobenzene unit **C** to weaken the binding affinity as in **9** makes the resultant pentamers more $Cs^+$-selective than **2b**, with increased $Cs^+$ extraction percentage from 37% for **2b** to 44% for **7**, 50% for **8**, and 51% for **9** (Figure 6a). Further calculation on the basis of the extraction data in Table S2 shows that this improved selectivity is remarkably accompanied by steadily decreasing extraction percentages for both $K^+$ and $Na^+$ ions. These lead to the extraction percentage ratios of $Cs^+$:$K^+$ and $Cs^+$:$Na^+$ increasing in the order of **2b** < **7** < **8** < **9** from 4.1 to 5.7, 7.0, and 9.9 and from 7.9 to 8.0, 11.7, and 12.1, respectively. The fact that extraction of $Cs^+$ is as much as 63% with undetectable extractions of both $K^+$ and $Na^+$ ions at 0.1 mM of **9** suggests actual ion selectivities against $K^+$ and $Na^+$ ions to be much higher than 9.9 and 12.1, respectively, and so a possible use of **9** for selectively removing radioactive $^{134}Cs$ and $^{137}Cs$ from contaminated seawater from Fukushima Daiichi nuclear disaster.[12] Curiously, the ability of **2b** to efficiently extract the second most extractable $Ba^{2+}$ ions is sharply aborted via a single "mutation" of unit **B** to either **A, C,** or **D**, while ions including $Tl^+$, $Rb^+$, and $Ag^+$ still remain extractable to a good extent by all the four pentamers **2b** and **7–9**. On the basis of the computationally determined structure for the partially hydrated **2b**·$Ba^{2+}$ complex (Figure S4a) and the poor electron-donating ability of the F atom in **9**, the inability of **9** to bind a $Ba^{2+}$ ion might imply that the bond strength of $Ba^{2+}$−O found in the pentamer·$Ba^{2+}$ complexes such as **2b**·$Ba^{2+}$ roughly lies within 80–100% of that of $Ba^{2+}$−O bond formed between the $Ba^{2+}$ ion and water molecules.
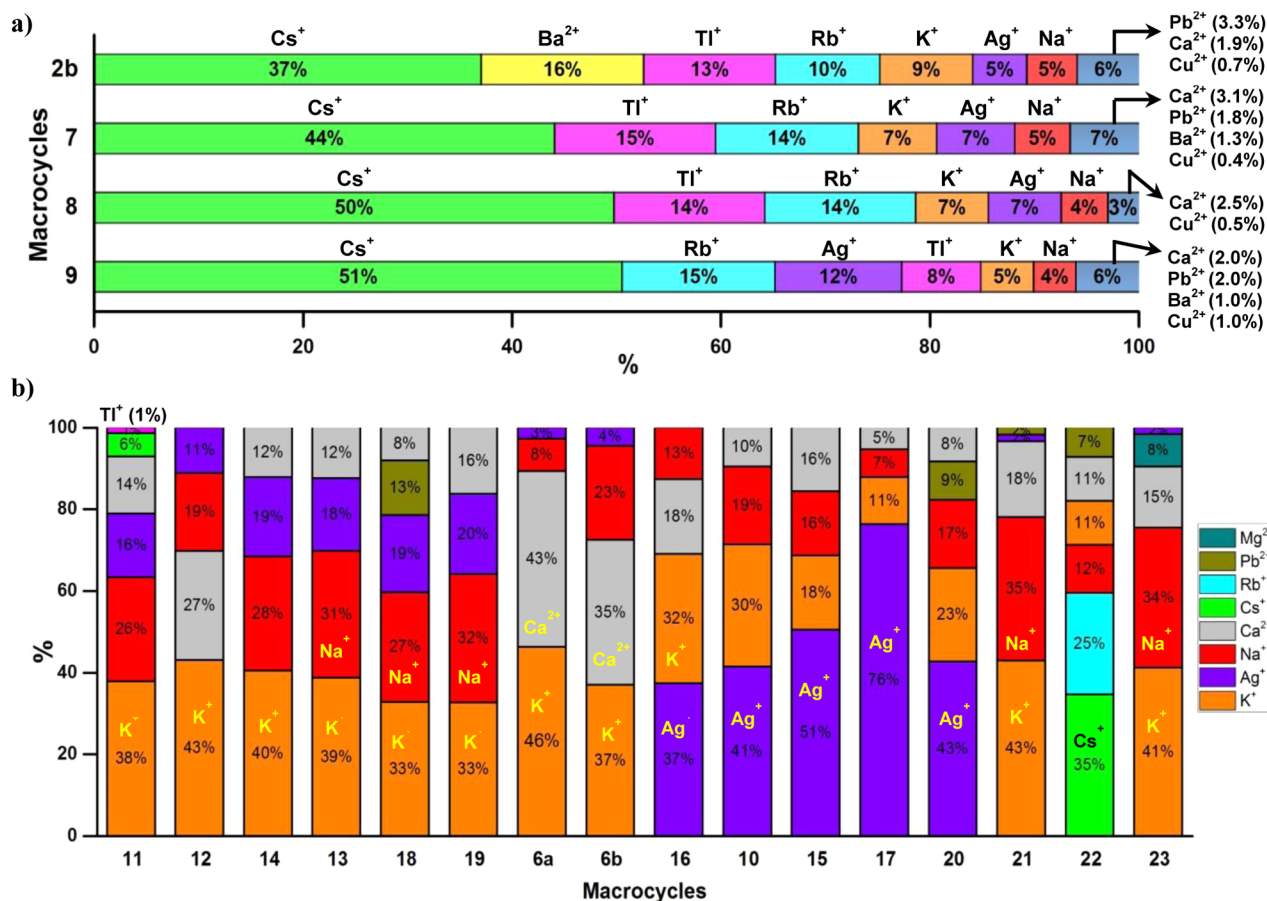
**Figure 6.** Schematic illustrations of ion-binding selectivities by macrocycles **2b** and **6−23**. A host is considered to have a dual selectivity if the extractability of the second most extractable ion lies within 80% of the most extractable one by the same host (Table S1). The most extractable ions and those ions whose extractability lies within 80% of the most extractable ones are additionally highlighted in the cavity to illustrate the ion-binding selectivity among the varying hosts.

For the other 13 pentamers **6** and **10−20** having two or more sterically hindered unit **A**s (Figure 6b), the most extractable ions are either K^{+} ions that occur in 8 cases or Ag^{+} ions in 5 cases, with the second most extractable ions being K^{+} ions in 5 cases, Na^{+} ions in 5 cases, and Ca^{2+} ions in 3 cases. Coincidentally, whereas the K^{+} ions are the second most extractable ions, the Ag^{+} ions, not Na^{+}, Ca^{2+}, or other ions, are always the most extractable ones, highlighting a possibly intrinsic ability of such sterically hindered pentameric framework to preferentially recognize K^{+} over all the other non-Ag^{+} ions. More generally but more narrowly, K^{+} ions appear to be intrinsically favored over many extractable ions such as Na^{+}, Ca^{2+}, Pb^{2+}, and Cu^{2+} ions by all the 17 pentameric hosts **2b** and **6−20**, while sterically much hindered **6** and **10−20** prefer K^{+}, Ag^{+}, Na^{+}, and Ca^{2+} over all the other ions. Except for K^{+}-selective **14**, the other three hydroxyl-containing pentamers **15−17** are all Ag^{+} selective. An interesting point to note is that all the Ag^{+}-selective pentamers (**10, 15−17**, and **20**) display a higher extraction capacity toward Ag^{+} ions than all the K^{+}-selective pentamers toward K^{+} ions (85−98% for Ag^{+} vs 59−82% for K^{+} at the host concentration of 0.6 mM, Table S1). Of high interest is pentamer **17**, which recognizes Ag^{+} ions in a high-affinity yet highly selective manner (e.g., a selectivity factor of 7 over K^{+} ions and excellent extraction efficiencies of 53% and 95% at the host concentrations of 0.1 and 0.3 mM, respectively, Figure 6b and Table S2). This unusually high affinity recognition and high capacity extraction of Ag^{+} ions

likely can be accounted for by the complexation-induced deprotonation of one of the three phenolic hydroxyl groups in **17** by the Ag^{+} ion.[10c]

Lastly, it might be worth further comparing with well-known ligands such as 18-crown-6 (**21**) and kryptonfix-222 (**23**). By using picrate extraction experiments developed by Cram,[13] pentamer **2b** was found to extract Li^{+}, Na^{+}, K^{+}, Rb^{+}, and Cs^{+} ions from aqueous solution into chloroform layer with extraction efficiencies of 94%, 95%, 88%, 95%, and 96%, respectively, while the corresponding extraction efficiencies are 0%, 11%, 81%, 74%, and 51% for 18-crown-6 and 23%, 94%, 93%, 97%, and 46% for kryptonfix-222. On the basis of these extraction data, the binding constants of **2b** toward these five alkali metal picrate salts (Li^{+}, Na^{+}, K^{+}, Rb^{+}, and Cs^{+}) were determined to be on the order of $10^9$ M$^{-1}$, which are much higher than those exhibited by 18-crown-6 and comparable to kryptonfix-222 (Table 2). Compared to 18-crown-6 that is more selective toward K^{+} and Rb^{+} ions and kryptonfix-222 that is highly selective toward Na^{+}, K^{+}, and Rb^{+} ions, pentamer **2b** turns out to be not very selective in ion binding toward alkali metal picrate salts. Nevertheless, by switching picrate to chloride salts and using the host concentration at 0.10 mM and each of the 20 metal ions at 0.03 mM (Table S2), **2b** is not only much more selective but also better in binding capacity than both 18-crown-6 and kryptonfix-222. More specifically, while **2b** becomes Cs^{+}-selective and is able to extract 62% of Cs^{+}, 26% of Ba^{2+}, 21% of Tl[+], 17% of Rb^{+}, and 13% of K^{+}, both

**Table 2. Binding Constants $K_a$ for 2b, 21, and 23 Complexing Alkali Picrate Salts From Li$^+$ to Cs$^+$ in H$_2$O/CHCl$_3$ at 10 mM at 25 °C Obtained by Cram's Method[13]**

| | $K_a$ (M$^{-1}$)[a] | | |
|---|---|---|---|
| picrate salt | 2b | 21 | 23 |
| Li$^+$ | $8.9 \times 10^9$ | 0 | $3.3 \times 10^6$ |
| Na$^+$ | $9.1 \times 10^9$ | $8.2 \times 10^5$ | $4.7 \times 10^9$ |
| K$^+$ | $7.2 \times 10^8$ | $2.4 \times 10^8$ | $2.0 \times 10^9$ |
| Rb$^+$ | $1.2 \times 10^9$ | $5.0 \times 10^7$ | $2.2 \times 10^9$ |
| Cs$^+$ | $4.4 \times 10^9$ | $7.1 \times 10^6$ | $4.8 \times 10^6$ |

[a]Averaged values over three runs with the assumption of 1:1 guest:host binding stoichiometry. All the binding constants have a relative error of ≤10%.

18-crown-6 and kryptonfix-222 are only able to extract three metal ions (Na$^+$, K$^+$, and Ca$^{2+}$) and incapable of discriminating K$^+$ from Na$^+$ ions with their corresponding extraction efficiencies toward Na$^+$, K$^+$, and Ca$^{2+}$ being 23%, 28%, and 12% for 18-crown-6 and 19%, 23%, and 10% for kryptonfix-222. Anomalously, kryptonfix-222 appears to possess a weaker, rather than stronger (Table 2), binding strength toward both K$^+$ and Na$^+$ ions in their chloride salts than 18-crown-6 across all the concentrations studied (Table S2).

**Structural Insights into the Pentamer−Metal Ion Complexes.** After many unsuccessful attempts, the X-ray quality crystals of (14)$_2$·K$^+$ were the only ones obtained by us, which were grown out using a four-layer technique involving extremely slow diffusion of top KNO$_3$-containing methanol layer successively into the second layer containing methanol, the third layer containing 1:1 mixed methanol and dichloromethane, and finally the bottom 14-containing dichloromethane layer over months at room temperature. In the crystal structure, two enantiomeric pentameric hosts can be found (Figure 7a), and the same two enantiomers sandwich a potassium ion to form a 2:1 complex (14)$_2$·K$^+$ (Figure 7b). In such complexes, K$^+$ ions are six-coordinated, sandwiched, and stabilized by two binding pockets, each formed by one strongly coordinating pyridone O atom (K$^+$···O distance = 2.67 Å) and two additional moderately strong coordination bonds (K$^+$···O−CH$_3$ distance = 3.15 Å and K$^+$···O=C distance = 3.02 Å). Due to the hydrophobic pushes from the two adjacent methyl groups with the shortest K$^+$···H−CH$_2$O distance of 3.35 Å, K$^+$ ions of 1.38 Å in radius would have to occupy an off-center position within the cavity similarly measuring 1.4 Å in radius. The interplanar distance between the two pentamer molecules of 14 in the complex is around 3.3 Å, suggesting a nice fit of potassium ion into the binding pocket that enables efficient aromatic π−π stacking to take place. This further suggests that larger cations such as Cs$^+$ and Rb$^+$ ions may be forced into the vicinity of the hydrophobic methyl groups in 14 and, in the meantime, may enlarge the interplanar distance that disfavors aromatic π−π stacking interactions. Consequently, sterically hindered pentamers containing two or more alkoxy groups of **A** or **D** are expected not to bind larger Cs$^+$ (1.67 Å) and Rb$^+$ (1.52 Å) ions, which is consistent with experimental data obtained on 6 and 10−20 (Figure 6c and Table S1). Instead, smaller ions such as K$^+$ (1.38 Å), Ag$^+$ (1.15 Å), Na$^+$ (1.02 Å), and Ca$^{2+}$ (1.15 Å) are preferred by these hosts. Structure-wise, we propose that all the 11 structurally similar pentameric hosts 10−20 form a 2:1 sandwiched structure with K$^+$ ions. In the case of Ag$^+$ (1.15 Å), Na$^+$ (1.02 Å), and Ca$^{2+}$ (1.15 Å), 1:1 complexes should be formed since (1) these smaller cations
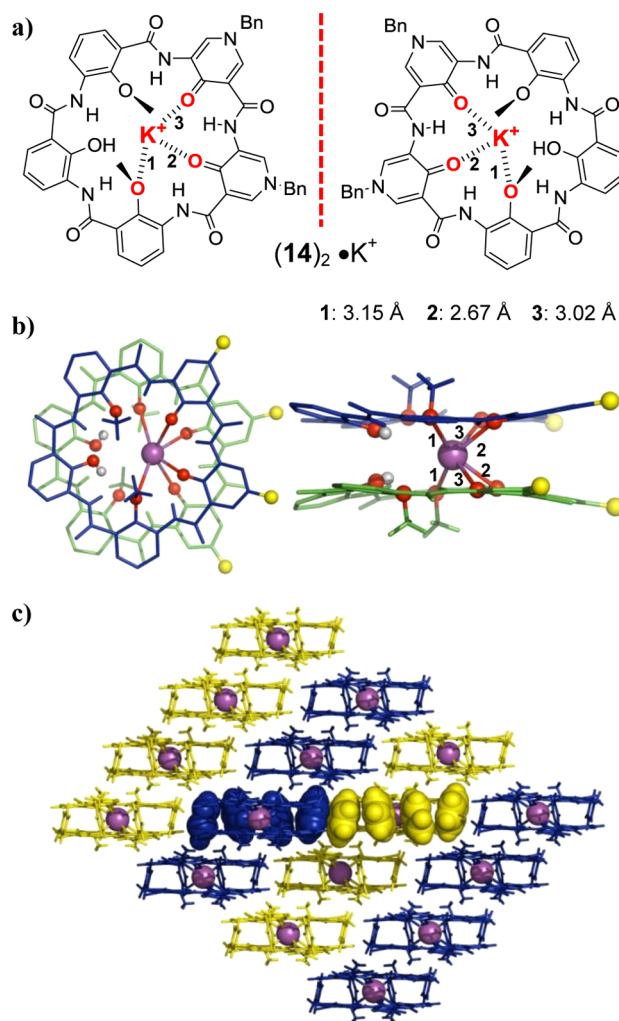


**1**: 3.15 Å   **2**: 2.67 Å   **3**: 3.02 Å

**Figure 7.** Crystal structure and 2D molecular packing of a K$^+$-containing complex (14)$_2$·K$^+$. (a) A pair of enantiomeric complexes exist in the solid state. (b) Top and side views of the complex made up of two identical enantiomeric pentamers. (c) Molecular packing involving the two enantiomeric complexes highlighted in yellow and blue, respectively. In (b), the yellow atoms refer to the benzyl groups.

actually prefer to stay in an off-center position as inferred from the computationally determined structures using pentamer **2b** (Figure 8b−d) and (2) formation of 2:1 sandwiched structure would shorten the interplanar distance of ~3.3 Å observed in the crystal structure of (14)$_2$·K$^+$, thereby disfavoring aromatic π−π stacking interactions. Due to the presence of three hydrophobic groups occupying both sides of the pentameric plane (Figure 4), both hosts **6a** and **6b** highly likely form only 1:1 complexes with all the recognizable metal ions.

The facts that smaller metal ions such as Ba$^{2+}$, K$^+$, Ag$^+$, Na$^+$, and Ca$^{2+}$ and larger Rb$^+$ ions all are computationally found to occupy the cavity center of **2b** and stay coplanar with the pentameric backbone in **2b** and that the Tl$^+$ ion deviates vertically from the pentameric plane by only 0.8 Å strongly suggest the formation of 1:1 complexes between these metal ions and hosts **2b** and **7−9** (Figure 8). In light of its computationally determined vertical deviation of about 2.0 Å from the slightly twisted pentameric plane in **2b** (Figure 8e) and depending on its concentration, Cs$^+$ ion expectedly is able to form both 1:1 and 2:1 sandwiched complexes with hosts **2b** and **7−9**. Structural optimization of a 2:1 sandwiched complex
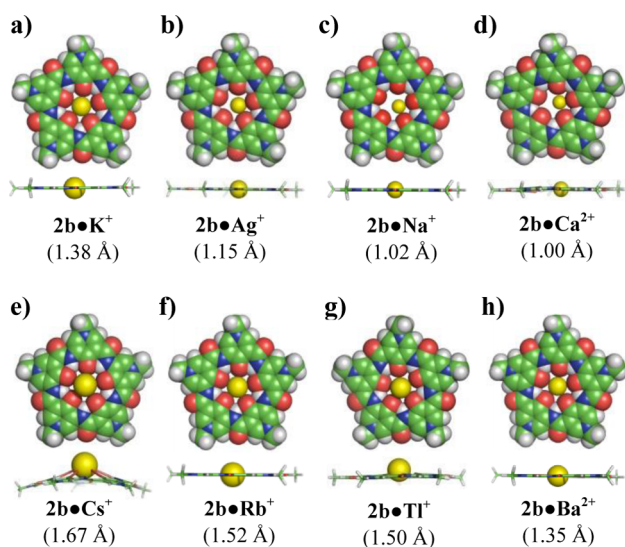
**Figure 8.** Computationally optimized structures of partially hydrated $2b \cdot [M(H_2O)_n]^{m+}$ ($n = 2$ or $3$ and $m = 1$ or $2$) complexes containing two or three axially coordinated water molecules at the level of B3LYP/6-31G(d,p) in chloroform. All the CPK models were built based on the van der Waals radius (gray: H = 1.20 Å; green: C = 1.70 Å; blue: N = 1.55 Å; red: O = 1.52 Å). The yellow atoms in all the structures refer to metal cations whose radii were specified in the respective parentheses. In all the structures except for $2b \cdot [Cs(H_2O)_3]^+$ (e) for which three water molecules on the same side were included in the computation, the metal ions are assumed to be six-coordinated, and all the coordinated water molecules have been removed for clarity of view. From the calculated structures where most of the metal ions stay coplanar with the planar pentameric backbone, it can be seen that the cavity in $2b$ is too small for both $Cs^+$ and $Tl^+$ ions that are above the slightly twisted pentameric planes by about 2.0 and 0.8 Å, respectively, just right for $K^+$, $Rb^+$, and $Ba^{2+}$ ions and slightly too big for $Ag^+$, $Na^+$, and $Ca^{2+}$ ions.

$(2b)_2 \cdot Cs^+$ reveals an interplanar distance of 3.8 Å (Figure S4b), which is close to the typical aromatic $\pi-\pi$ distance of 3.4 Å.

### CONCLUSION

We have demonstrated here a novel foldamer-based macrocyclic system for combinatorially constructing modularly tunable macrocyclic hybrid pentamers of diverse structures. These hybrid pentamers are uniquely characterized by having a H-bond-rigidified shape-persistent near-planar pentameric skeleton that effectively and convergently preorganizes differential electronic traits (e.g., O and F atoms) and influential steric/hydrophobic (e.g., methyl and ethyl groups) factors into an ultrasmall yet adjustable cavity of up to 1.4 Å in radius, thereby permitting a systematic and combinatorial evolution of circular pentamers with an ability to selectively recognize $Cs^+$, $K^+$, or $Ag^+$ ions in the presence of 19 other metal ions. The wealth and diversity of circularly folded hybrid pentamers sensible from their large sequence space upon additional incorporations of pyridine N-oxides, sulfanes,[11a] thiol groups, or halogen atoms[11c] into the same pentameric framework[11b] open up a whole new dimension of scientific research, encompassing enormous complexation/inclusion capacities from which the best complementary binding motif responding to a specific metal ion of interest may be identified. Further exquisite modifications and ensuring applications of these cavity-containing ion-binding circular synthons should offer

wider perspectives and achievements that have not been made possible before.

### ASSOCIATED CONTENT

**Ⓢ Supporting Information**

The Supporting Information is available free of charge on the ACS Publications website at DOI: 10.1021/jacs.5b07123.

> Synthetic procedures for **5−20** as well as a full set of characterization data including $^1H$ NMR, $^{13}C$ NMR, (HR)MS, X-ray crystal file/data sheet for **2b, 5, 6,** and **14**, ICP data for **2** and **6−23**, and computational details (PDF)
>
> Crystallographic data (TXT)

### AUTHOR INFORMATION

**Corresponding Author**
*hqzeng@ibn.a-star.edu.sg

**Author Contributions**
⊥These authors contributed equally.

**Notes**
The authors declare no competing financial interest.

### REFERENCES

(1) (a) Pedersen, C. J. *J. Am. Chem. Soc.* **1967**, *89*, 2495. (b) Pedersen, C. J. *J. Am. Chem. Soc.* **1967**, *89*, 7017. (c) Dietrich, B.; Lehn, J.-M.; Sauvage, J.-P. *Tetrahedron Lett.* **1969**, *10*, 2885. (d) Dietrich, B.; Lehn, J.-M.; Sauvage, J.-P. *Tetrahedron Lett.* **1969**, *10*, 2889. (e) Cram, D. J.; Kaneda, T.; Helgeson, R. C.; Lein, G. M. *J. Am. Chem. Soc.* **1979**, *101*, 6752. (f) Trueblood, K. N.; Knobler, C. B.; Maverick, E.; Helgeson, R. C.; Brown, S. B.; Cram, D. J. *J. Am. Chem. Soc.* **1981**, *103*, 5594.

(2) (a) Hamuro, Y.; Geib, S. J.; Hamilton, A. D. *Angew. Chem., Int. Ed. Engl.* **1994**, *33*, 446. (b) Yuan, L.-H.; Feng, W.; Yamato, K.; Sanford, A. R.; Xu, D.; Guo, H.; Gong, B. *J. Am. Chem. Soc.* **2004**, *126*, 11120. (c) Ferguson, J. S.; Yamato, K.; Liu, R.; He, L.; Zeng, X. C.; Gong, B. *Angew. Chem., Int. Ed.* **2009**, *48*, 3150. (d) Li, Z. T.; Hou, J. L.; Li, C.; Yi, H. P. *Chem. - Asian J.* **2006**, *1*, 766. (e) Ong, W. Q.; Zeng, H. Q. *J. Inclusion Phenom. Mol. Recognit. Chem.* **2013**, *76*, 1. (f) Fu, H. L.; Liu, Y.; Zeng, H. Q. *Chem. Commun.* **2013**, *49*, 4127.

(3) For some selected reviewers in foldamers, see: (a) Gellman, S. H. *Acc. Chem. Res.* **1998**, *31*, 173. (b) Hill, D. J.; Mio, M. J.; Prince, R. B.; Hughes, T. S.; Moore, J. S. *Chem. Rev.* **2001**, *101*, 3893. (c) Gong, B. *Acc. Chem. Res.* **2008**, *41*, 1376. (d) Saraogi, I.; Hamilton, A. D. *Chem. Soc. Rev.* **2009**, *38*, 1726. (e) Guichard, G.; Huc, I. *Chem. Commun.* **2011**, *47*, 5933. (f) Zhang, D.-W.; Zhao, X.; Hou, J.-L.; Li, Z.-T. *Chem. Rev.* **2012**, *112*, 5271.

(4) (a) Shirude, P. S.; Gillies, E. R.; Ladame, S.; Godde, F.; Shin-Ya, K.; Huc, I.; Balasubramanian, S. *J. Am. Chem. Soc.* **2007**, *129*, 11890. (b) Helsel, A. J.; Brown, A. L.; Yamato, K.; Feng, W.; Yuan, L. H.; Clements, A. J.; Harding, S. V.; Szabo, G.; Shao, Z. F.; Gong, B. *J. Am. Chem. Soc.* **2008**, *130*, 15784. (c) Sanford, A. R.; Yuan, L. H.; Feng, W.; Flowersb, K. Y. R. A.; Gong, B. *Chem. Commun.* **2005**, 4720. (d) Qin, B.; Ren, C. L.; Ye, R. J.; Sun, C.; Chiad, K.; Chen, X. Y.; Li, Z.; Xue, F.; Su, H. B.; Chass, G. A.; Zeng, H. Q. *J. Am. Chem. Soc.* **2010**, *132*, 9564. (e) Ren, C. L.; Maurizot, V.; Zhao, H. Q.; Shen, J.; Zhou, F.; Ong, W. Q.; Du, Z. Y.; Zhang, K.; Su, H. B.; Zeng, H. Q. *J. Am. Chem. Soc.* **2011**, *133*, 13930. (f) Shen, J.; Ma, W. L.; Yu, L.; Li, J.-B.; Tao, H.-C.; Zhang, K.; Zeng, H. Q. *Chem. Commun.* **2014**, *50*, 12730. (g) Hu, J.; Chen, L.; Ren, Y.; Deng, P.; Li, X.; Wang, Y.; Jia, Y.; Luo, J.; Yang, X.; Feng, W.; Yuan, L. *Org. Lett.* **2013**, *15*, 4670. (h) Jiang, H.; Leger, J.-M.; Guionneau, P.; Huc, I. *Org. Lett.* **2004**, *6*,

2985. (i) Zhu, Y. Y.; Li, C.; Li, G. Y.; Jiang, X. K.; Li, Z. T. *J. Org. Chem.* **2008**, *73*, 1745. (j) Ren, C. L.; Xu, S. Y.; Xu, J.; Chen, H. Y.; Zeng, H. Q. *Org. Lett.* **2011**, *13*, 3840. (k) Zhao, H. Q.; Shen, J.; Guo, J. J.; Ye, R. J.; Zeng, H. Q. *Chem. Commun.* **2013**, *49*, 2323. (l) Qin, B.; Jiang, L. Y.; Shen, S.; Sun, C.; Yuan, W. X.; Li, S. F. Y.; Zeng, H. Q. *Org. Lett.* **2011**, *13*, 6212.

(5) (a) Qin, B.; Chen, X. Y.; Fang, X.; Shu, Y. Y.; Yip, Y. K.; Yan, Y.; Pan, S. Y.; Ong, W. Q.; Ren, C. L.; Su, H. B.; Zeng, H. Q. *Org. Lett.* **2008**, *10*, 5127. (b) Ren, C. L.; Zhou, F.; Qin, B.; Ye, R. J.; Shen, S.; Su, H. B.; Zeng, H. Q. *Angew. Chem., Int. Ed.* **2011**, *50*, 10612.

(6) (a) Qin, B.; Ong, W. Q.; Ye, R. J.; Du, Z. Y.; Chen, X. Y.; Yan, Y.; Zhang, K.; Su, H. B.; Zeng, H. Q. *Chem. Commun.* **2011**, *47*, 5419. (b) Du, Z. Y.; Ren, C. L.; Ye, R. J.; Shen, J.; Lu, Y. J.; Wang, J.; Zeng, H. Q. *Chem. Commun.* **2011**, *47*, 12488. (c) Fu, H. L.; Chang, H.; Shen, J.; Lu, Y.-J.; Qin, B.; Zhang, K.; Zeng, H. Q. *Chem. Commun.* **2014**, *50*, 3582.

(7) (a) Cram, D. J.; Kaneda, T.; Helgeson, R. C.; Lein, G. M. *J. Am. Chem. Soc.* **1979**, *101*, 6752. (b) Sessler, J. L.; Seidel, D. *Angew. Chem., Int. Ed.* **2003**, *42*, 5134. (c) Pareek, Y.; Ravikanth, M.; Chandrashekar, T. K. *Acc. Chem. Res.* **2012**, *45*, 1801. (d) Zhang, W.; Moore, J. S. *Angew. Chem., Int. Ed.* **2006**, *45*, 4416. (e) Borisova, N. E.; Reshetova, M. D.; Ustynyuk, Y. A. *Chem. Rev.* **2007**, *107*, 46. (f) Lee, S.; Chen, C.-H.; Flood, A. H. *Nat. Chem.* **2013**, *5*, 704.

(8) X-ray quality crystals for pentamer **2a** were obtained by slow diffusion of cyclohexane into dichloromethane over a few weeks at room temperature.

(9) The crescent shape is used here to deduce the likely backbone curvature inducible by multiple units **E** that are to be incorporated into a circularly folded pentamer and are rigidified by the macrocyclic ring constraint to take up a crescent shape. But do note that these acyclic oligomers consisting of multiple units **E** will not adopt a crescent shape similar to that of $(\mathbf{B})_3$. Instead, the acyclic oligomers $(\mathbf{E})_n$ will take a linear geometry via alternative H-bonds formed between amide carbonyl O- and H-atom of the phenolic hydroxyl group. See ref 10b.

(10) (a) Yan, Y.; Qin, B.; Ren, C. L.; Chen, X. Y.; Yip, Y. K.; Ye, R. J.; Zhang, D. W.; Su, H. B.; Zeng, H. Q. *J. Am. Chem. Soc.* **2010**, *132*, 5869. (b) Sun, C.; Ren, C. L.; Wei, Y. C.; Qin, B.; Zeng, H. Q. *Chem. Commun.* **2013**, *49*, 5307.

(11) (a) Tang, H.; Doerksen, R. J.; Jones, T. V.; Klein, M. L.; Tew, G. N. *Chem. Biol.* **2006**, *13*, 427. (b) Zhu, Y.-Y.; Yi, H.-P.; Li, C.; Jiang, X.-K.; Li, Z.-T. *Cryst. Growth Des.* **2008**, *8*, 1294. (c) Please see Figure S3 for additional building blocks **F−M** that could be potentially useful for constructing macrocyclic hybrid pentamers and for fine-tuning ion-binding affinity and selectivity. Nevertheless, our preliminary results show that synthesis of these monomeric building blocks such as pyridone N-oxide and their subsequent incorporation into the pentameric framework turned out to be synthetically very challenging, and we are currenlty working to improve and optimize the synthetic methdologies. For instance, even thought monomeric unit **F** can now be synthesized satisfactorily in our laboratory, for some unknown reasons, it is very troublesome to couple two or more **F** units or couple one unit of **F** with other units such as **A** to make a dimer or higher oligomers as such amide coupling steps tend to give very low yields.

(12) Brumfiel, G. *Nature News Blog* **2011**, http://blogs.nature.com/news/2011/09/directly_comparing_fukushima_t.html.

(13) Moore, S. S.; Tarnowski, T. L.; Newcomb, M.; Cram, D. J. *J. Am. Chem. Soc.* **1977**, *99*, 6398.